Measurement of timing resolution of the IceCube digital optical modules

Dmitry Chirkin, Robert Stokstad

dchirkin@lbl.gov

LBNL, USA

Abstract

During the fall of 2004 a number of tests were performed in the dark freezer lab (DFL) at University of Wisconsin at Madison (UWM) as part of the final acceptance testing (FAT) of the assembled digital optical modules (DOMs). An important test was performed with 1.5 kHz laser pulses, each of width ≈ 75 ps, fed into the DOMs by means of optical fibers and beam splitters. The optical occupancy of a single laser pulse per DOM was maintained at ≈ 0.1 to ensure that the majority of signal came from single photo-electron (SPE) events. In order to record the exact time when the laser fired the electrical pulse from the laser was fed directly into a DOM mainboard. In this report data from a set collected from 94 DOMs connected to the digital acquisition system (test DAQ) was used. This set consisted of 46 (unterminated) DOMs connected through shorter cables, 46 (terminated) DOMs connected through longer cables, one "reference" DOM run at room temperature, and a "laser" board. The cable length was simulated with shaping electronics, so while the measured roundtrip time of the time calibration packets corresponds to a couple hundred meters, the shape of signal after propagating through the simulated cable looks like that after propagating through some couple thousand meters of IceCube cable. Measuring the recorded time of the signal from DOMs correlated with laser pulses allows one to determine the extent of the uncertainty in this time, i.e., time resolution achievable with the setup described here.

It is shown that the requirement of 7 ns is well achieved allowing for plenty of leeway for other uncertainties, which may arise after the DOMs are deployed. Time calibration runs already made with the full IceCube cable at the time of writing of this report demonstrate that the achieved time resolution is as good, if not better than that measured with the simulated cable.

Contents

1 Introduction

The dataset analyzed in this report was that taken on 09/15/04, run 2141, designated as TimeResolution-ATWD0. The dataset consists of a configuration file (.xml), 94 DOM calibration files, monitoring stream (.mon), time calibration stream (.tcal), and data stream (.hit). These together occupy together 1.4 Gb, the data stream taking most of the space (98 %).

As shown in Figure 1, the dataset describes approximately 200 seconds of data. Figure 2 shows 1 second of data. The apparent "dashed" pattern of the data is attributed to the limitations of the algorithm used to retrieve the data (DOMHUB-APP) and software run on the DOM (DOM-APP), which become apparent at high enough data rates. Figure 3 zooms into 10 ms of data; on this scale single events become visibly separated.

2 Reciprocal Active Pulsing time calibration (RapCal)

Each DOM contains a clock running at 40 MHz. To calibrate such a clock a pulse is sent from the DOM readout (DOR) card at the time $\mathrm{dor_{tx}}$ measured with the DOR card (see Figure 4). Although the DOR clock runs at 20 MHz, the signal is sent at the edge of the DOR clock cycle. Therefore the accuracy of the timestamp is determined mainly by the clock jitter estimated to be of the order 10 ps.

The rectangular pulse sent by the DOR card substantially changes shape after propagating through the cable. This pulse is recoded by the DOM communication analog-to-digital converter (Comm ADC) (see Figures 5 and 6) and time-stamped by the DOM clock ($\mathrm{dom_{rx}}$). Since the granularity of the DOM clock is 50 ns, it is necessary to refine the $\mathrm{dom_{rx}}$ value. This is achieved by reconstructing the offset of the recorded waveform from the point where it was time-stamped (the end of the waveform, beginning of the 48th bin). In this report we used four algorithms which rely on determining the position of certain "fiducial" points in the waveform.

All four methods first determine the baseline as the average over the first 19 samples in the Comm ADC waveform. After that, the leading edge intercept method (see Figures 5 and 6) fits a line to the rising edge of the pulse in the vicinity of the fastest ascent and defines the point of intersection of this line with the baseline as the fiducial point. The leading edge threshold method uses the point of intersection with the pulse half-height above the baseline instead. Centroid establishes the center of gravity of the pulse above the baseline. Lastly, the crossover method looks for the peak sample, thereby locating the starting bin of the downgoing portion of the waveform. Then it fits a line to the downgoing portion of the pulse in the vicinity of the intersection with the baseline, the intersection point of this line with the baseline being the fiducial point.

All four methods calculate the location of their corresponding fiducial points along the Comm ADC waveform (here denoted $\mathrm{d(wf_{dom})}$), which are assumed to be a constant time interval away from the waveform starting point. This assumption can be tested, e.g., by looking at the stability of the roundtrip times. By the following definition, the roundtrip time is the time elapsed from the moment the downgoing pulse is timestamped by the DOR card to the time location of the fiducial point calculated by the chosen method, plus the equivalent contribution from the upgoing pulse.

$$\mathrm{T_d + T_u = (dor_{rx} - d(wf_{dor}) - dor_{tx}) - (dom_{rx} - d(wf_{dom}) - dom_{tx})}$$

The roundtrip time defined this way differs from the time it takes a single harmonic of the pulse to travel down and up by a constant factor Δ_i ($i = 1, ..., 4$), which depends on a particular method used to find fiducial points.

Resulting roundtrip times obtained with four algorithms described above are shown in Figure 7. Separation between short and long cables is clearly visible; all four methods result in 222 ns separation, which for the signal propagation speed of 0.2 m/ns corresponds to 22.2 m (one way). Root mean squared (RMS) deviation from the mean of the roundtrip time is shown in Figure 8 along with the mean roundtrip time obtained with the method which showed the smallest RMS, the crossover method. The distribution of RMS for all DOMs is shown in Figure 9. The crossover and centroid methods result in precision of 1-2 ns, while leading edge methods produce larger values of 2-4 ns.

A moment of time t_c located halfway between the moment the pulse was sent by DOR card and the moment the return pulse reached the DOR card is exactly the same as the moment of time located halfway between the moment the pulse reached DOM and the moment the return pulse was sent by DOM. A crucial assumption made here is that the time calibration-pulse propagation speed is the same when propagating up or down the cable. It is therefore important that the shape of the pulse sent by the DOR card is as close as possible to that sent by the DOM. Other factors which affect the up/down symmetry are extent of the cable asymetry, and effect of asymetrical temperature distribution along the cable.

The moment of time t_c can therefore be evaluated in terms of times measured by the DOR card clock and, independently, by the DOM internal clock:

$$t_{c,\mathrm{dor}} = \left(\mathrm{dor}_{\mathrm{tx}} + \mathrm{dor}_{\mathrm{rx}} - \mathrm{d}(\mathrm{wf}_{\mathrm{dor}}) - \Delta_i\right)/2, \quad \text{on the DOR side, and}$$

$$t_{c,\mathrm{dom}} = \left(\mathrm{dom}_{\mathrm{tx}} + \mathrm{dom}_{\mathrm{rx}} - \mathrm{d}(\mathrm{wf}_{\mathrm{dom}}) - \Delta_i\right)/2, \quad \text{on the DOM side.}$$

This allows one to calculate the *time delta* δ_t, defined as the time offset that must be added to the time measured by the DOM clock in order to get the corresponding time measured by the DOR card clock. At the moment of time t_c,

$$\delta_t = t_{c,\mathrm{dor}} - t_{c,\mathrm{dom}} = \left(\mathrm{dor}_{\mathrm{tx}} + \mathrm{dor}_{\mathrm{rx}} - \mathrm{d}(\mathrm{wf}_{\mathrm{dor}})\right)/2 - \left(\mathrm{dom}_{\mathrm{tx}} + \mathrm{dom}_{\mathrm{rx}} - \mathrm{d}(\mathrm{wf}_{\mathrm{dom}})\right)/2.$$

As seen from this equation, δ_t does not depend on Δ_i. The value of δ_t is calculated at the moment of time t_c, whose evaluated value depends on Δ_i. However, this dependence manifests itself only as an additive factor $-\Delta_i/2$ and can be consistently omitted for slowly varying functions $\delta_t(t_{c,\mathrm{dom}})$.

The value of δ_t determined this way as the function of t_c is shown in Figure 10. It is also possible to calculate the DOM clock frequency drift as compared to DOR card clock, shown in Figure 11 for a typical DOM. The apparent DOR-DOM frequency mismatch for this DOM is on average 0.428 μs/s, showing a frequency drift as large as 0.5 ns/s. Between the consecutive time calibration events (10 second apart for the dataset analyzed here) this translates into a clock drift of as much as 5 ns.

The function $\delta_t(t_{\mathrm{dom}})$ for t_{dom} values other than $t_{c,\mathrm{dom}}$ obtained during calibration cycles can be extrapolated from values of the two preceding time calibration events (as currently implemented in the data-collector) or interpolated from values of several surrounding time calibration events (as planned for the string processor). During stable run conditions as few as two surrounding time calibration events are sufficient to obtain the interpolate the function $\delta_t(t_{\mathrm{dom}})$. However, when run conditions are changing (e.g., warming up at the beginning of the run) three time calibrations may be necessary to account for unsettled DOM clock drifts. At the moment only polynomial interpolations, i.e., linear and 3-point parabola, are foreseen. A calculated correspondence of the time measured by DOM to *global time* (time at DOR card) obtained by linear interpolation is shown in Figure 12.

3 ATWD waveform feature extraction

4 Laser time resolution

5 Final acceptance test (FAT) data reader software

A Figures

List of Figures

A.1 Introduction and datasets

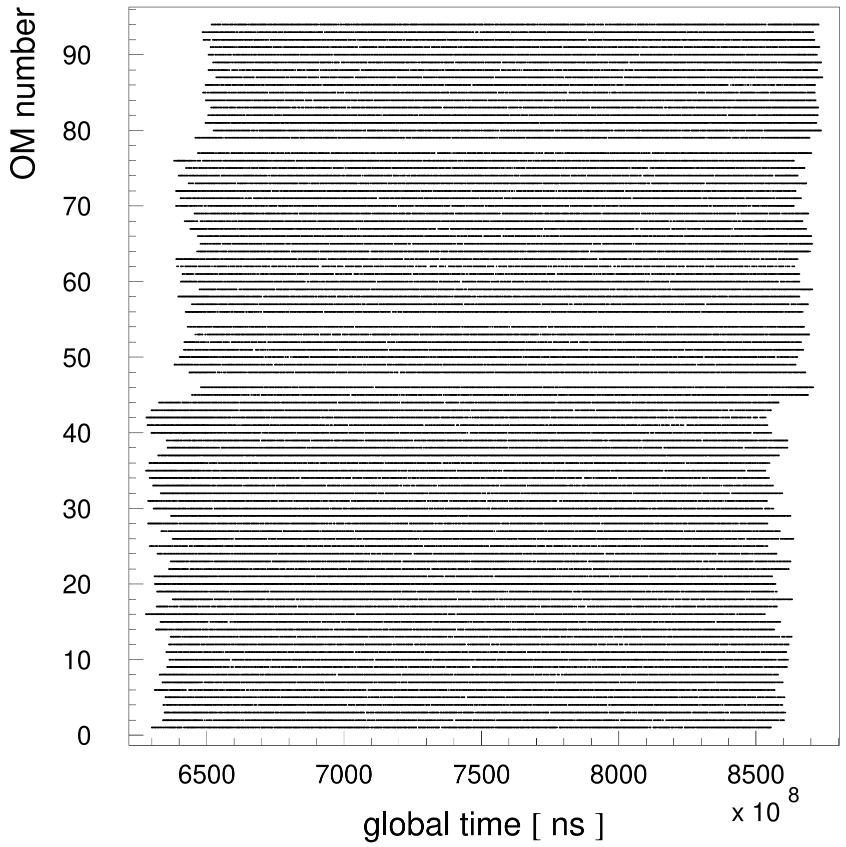

Figure 1: All of the data taken in run 2141: 94 DOMs, $\approx$ 200 seconds

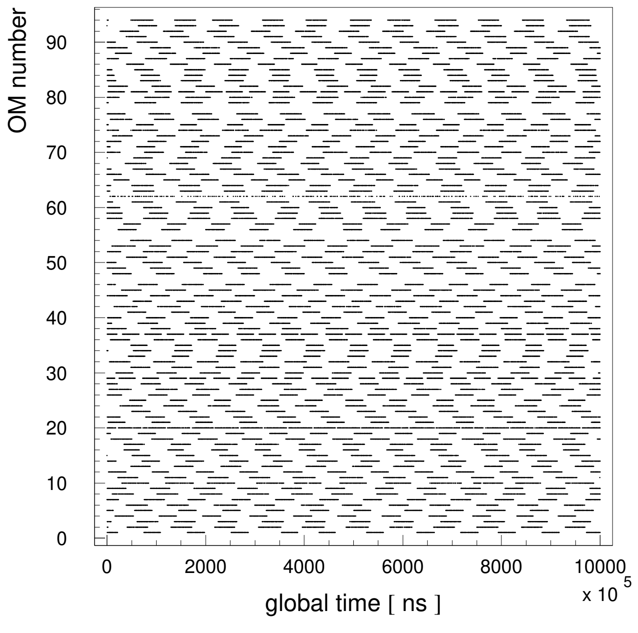

Figure 2: 1 second of data

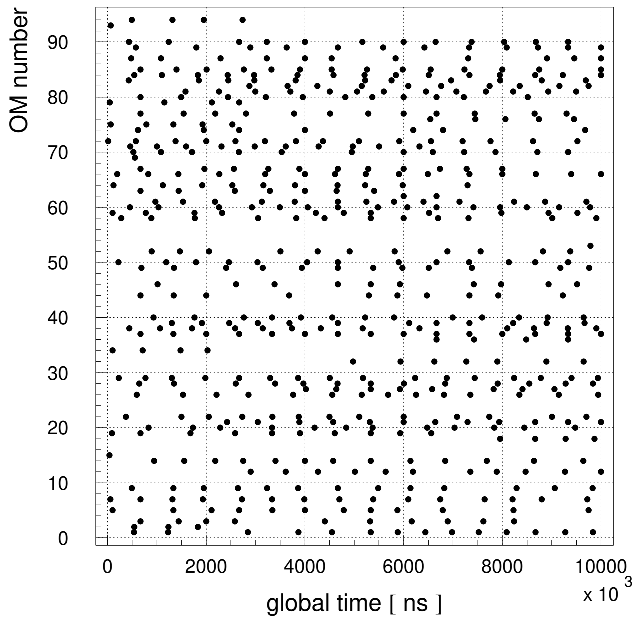

Figure 3: 10 ms of data

A.2 Reciprocal Active Pulsing time calibration (RapCal)

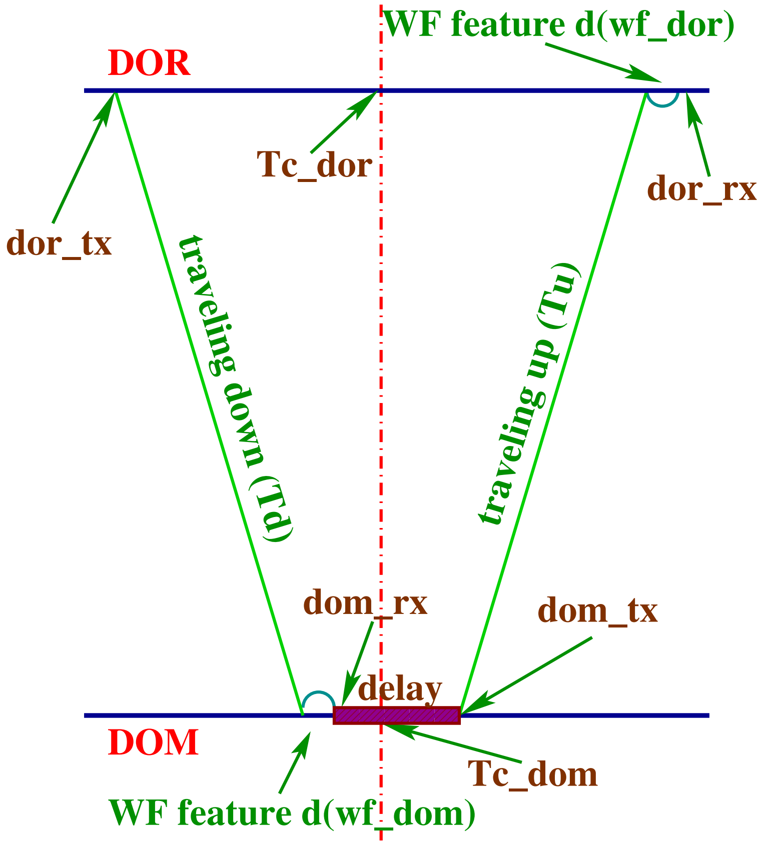

Figure 4: RapCal timing algorithm diagram

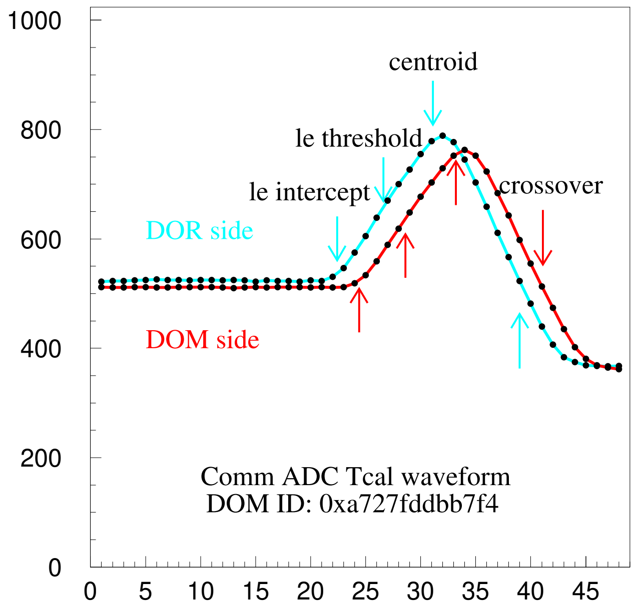

Figure 5: Tcal waveform for regular DOM

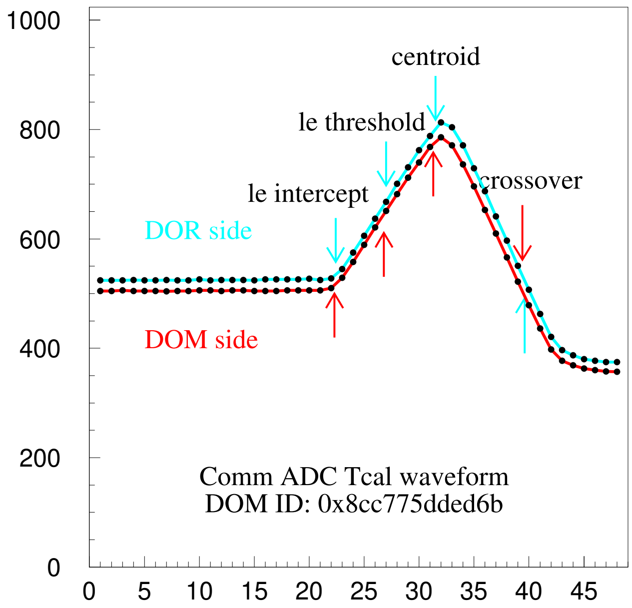

Figure 6: Tcal waveform for laser-board DOM

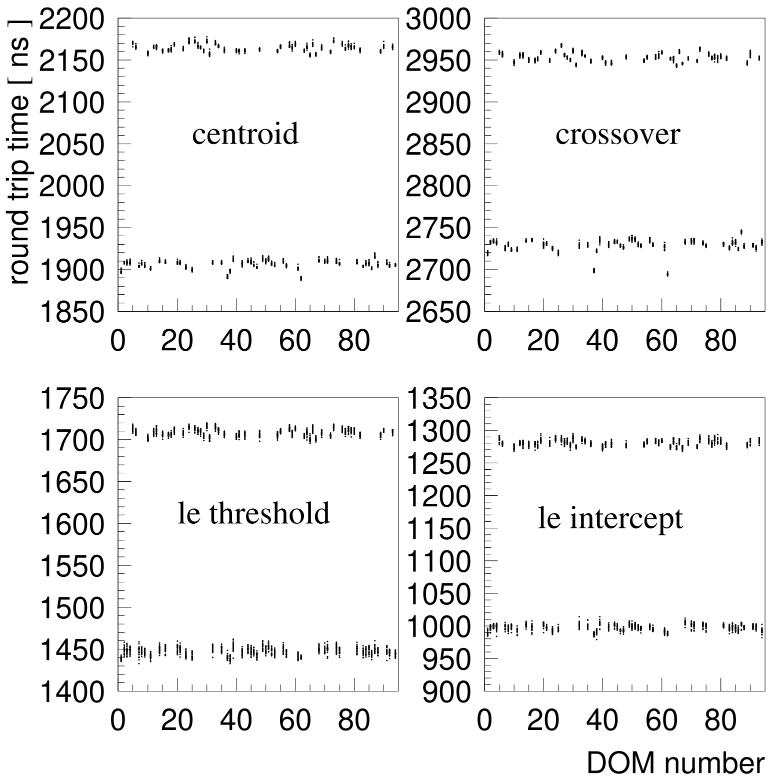

Figure 7: Round trip time measured with four methods

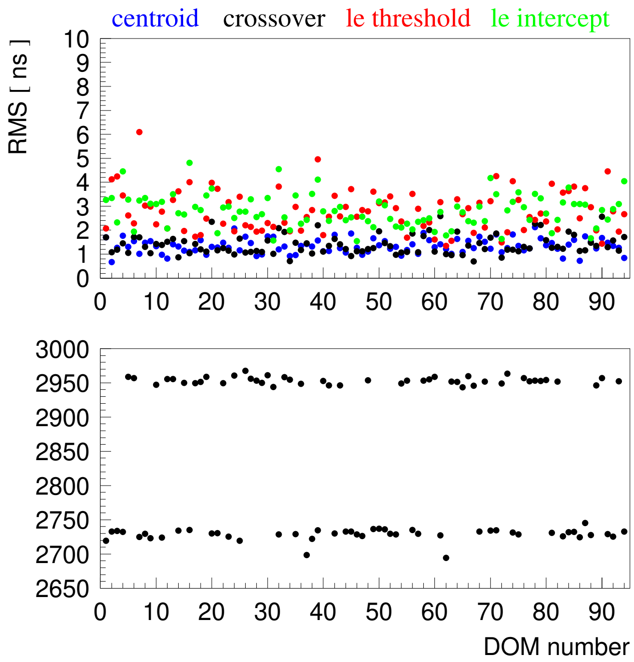

Figure 8: Width of the round trip time distributions (upper plot), average round trip time measured with crossover algorithm (lower plot)

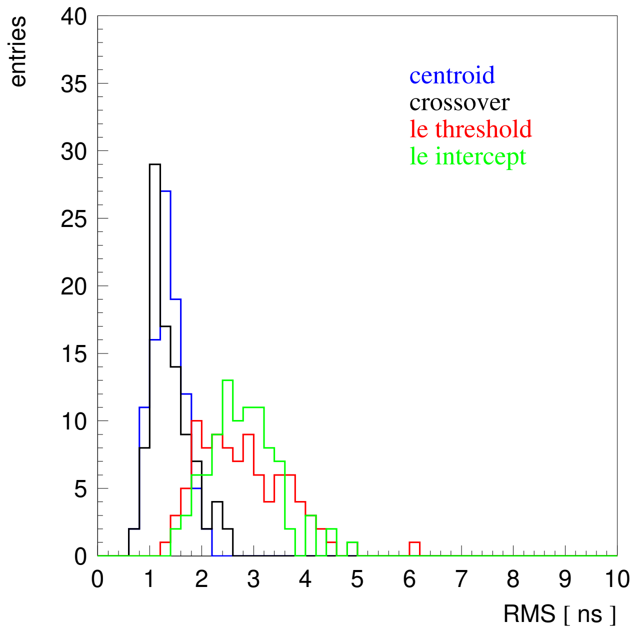

Figure 9: Round trip time RMS distribution

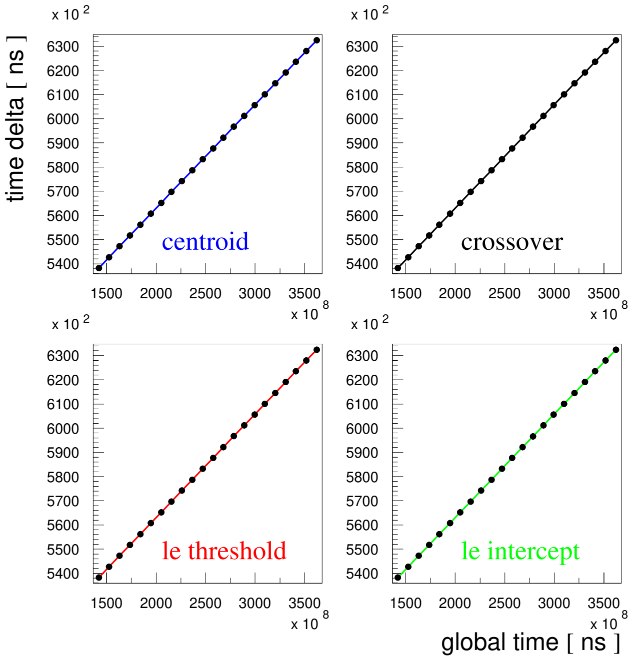

Figure 10: DOR-DOM clock time difference

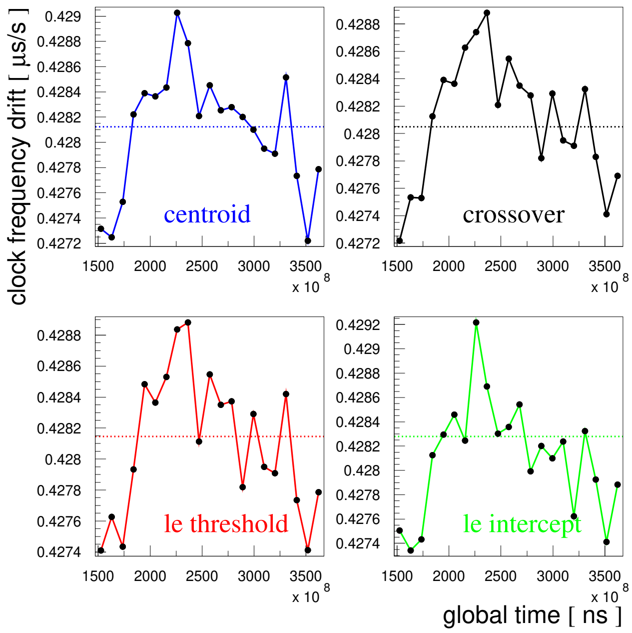

Figure 11: DOM clock frequency drift

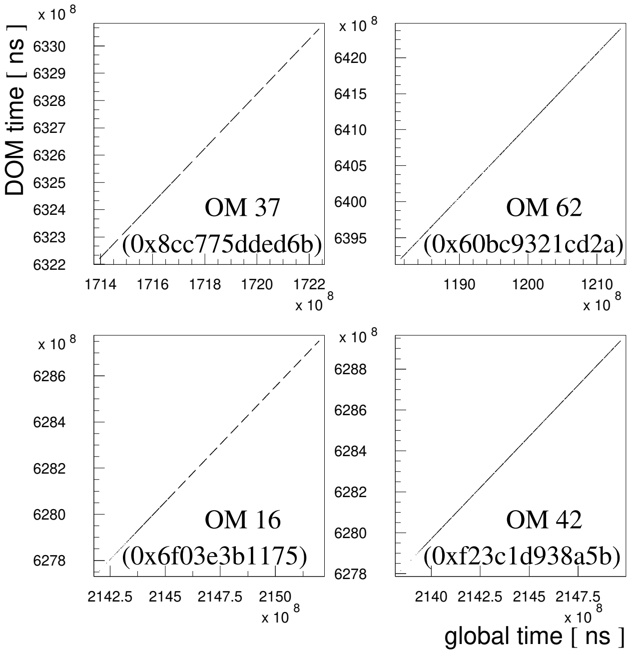

Figure 12: Global time of the hit events

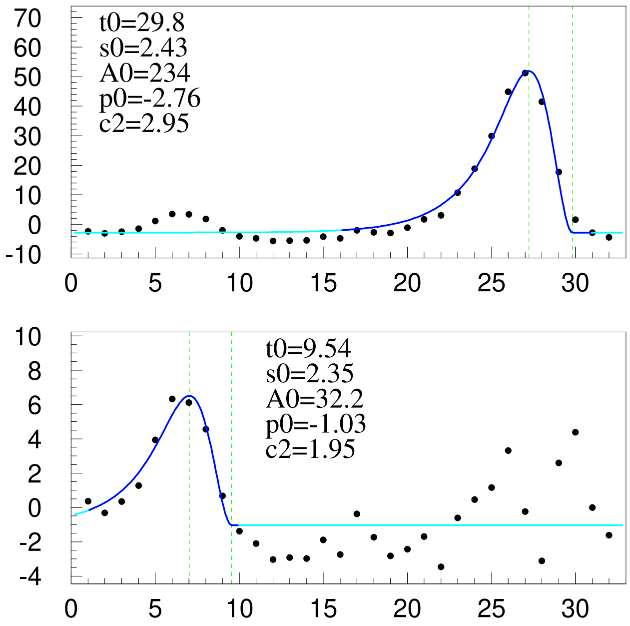

Figure 13: ATWD feature extraction algorithm

A.3 ATWD waveform feature extraction

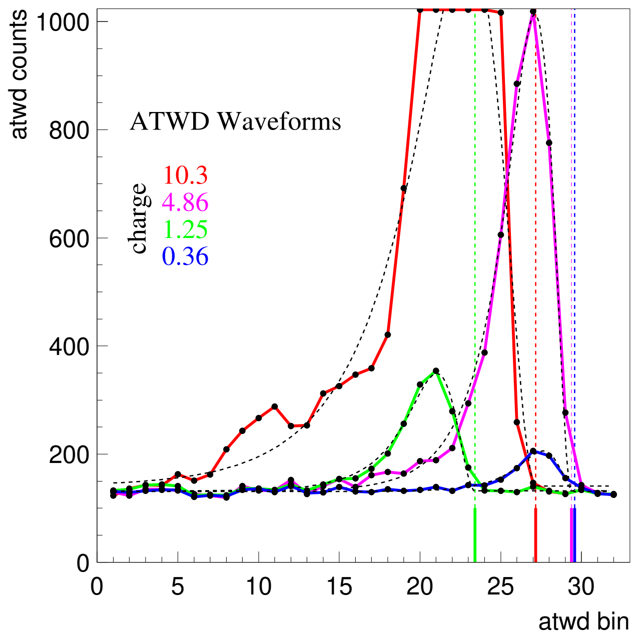

Figure 14: ATWD feature extraction for PMT pulses

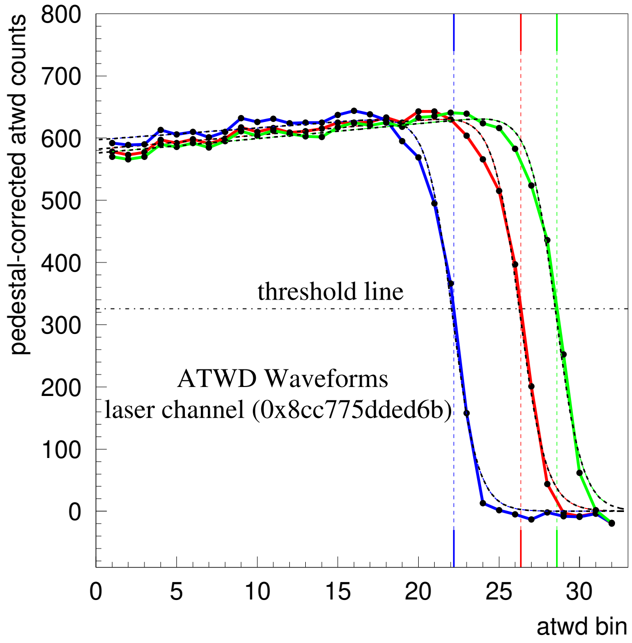

Figure 15: ATWD feature extraction for laser-board pulses

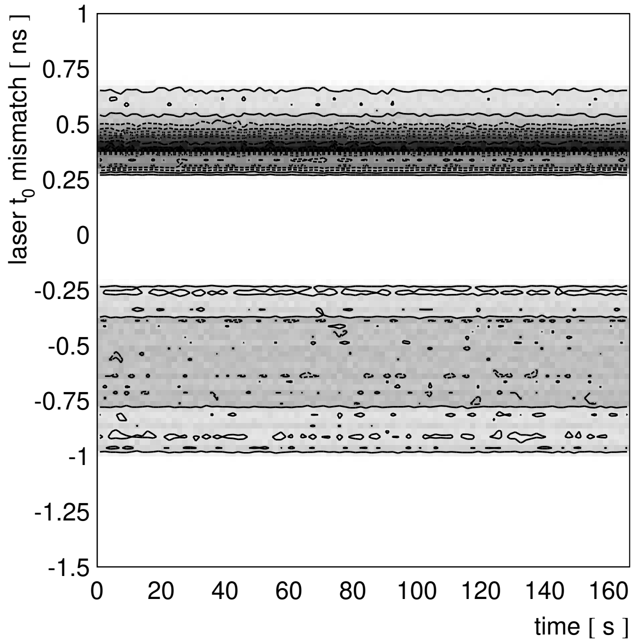

Figure 16: Laser pulse reconstructed t_0 mismatch: tanh * exp fit above, atan fit below

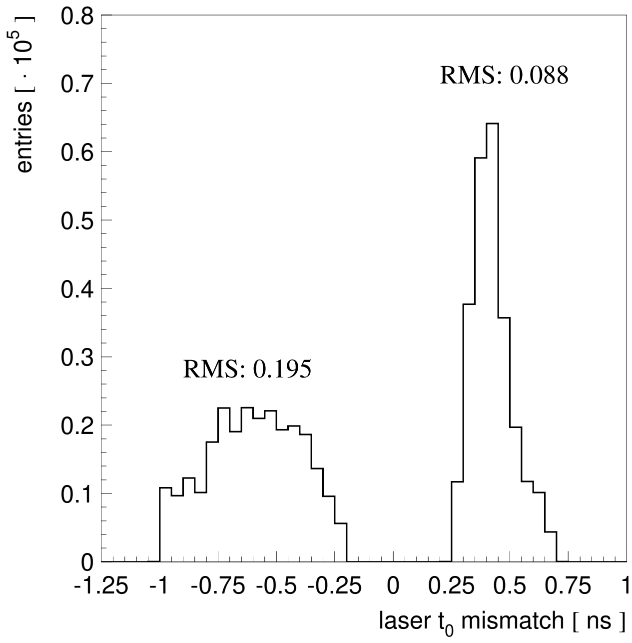

Figure 17: Laser t_0 mismatch distribution: tanh * exp fit (right) and atan fit (left)

A.4 Laser time resolution

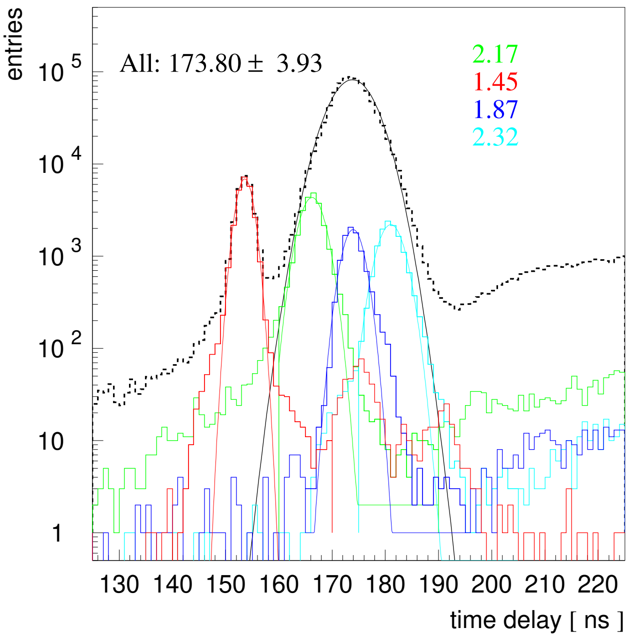

Figure 18: Laser time resolution: centroid

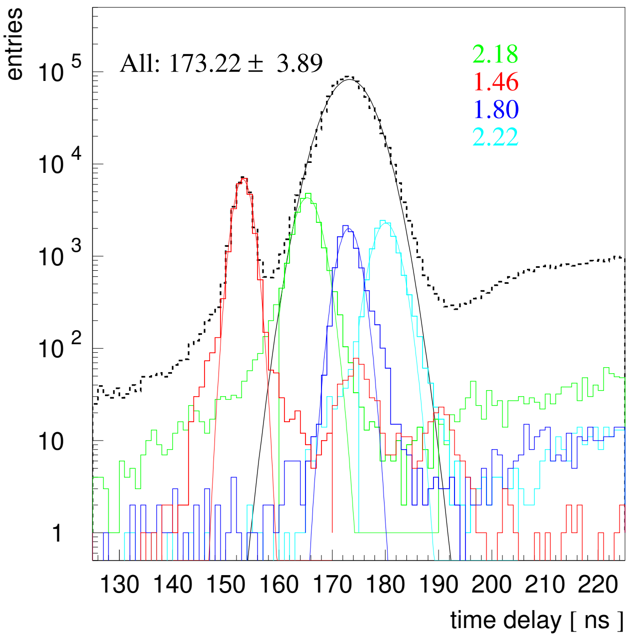

Figure 19: Laser time resolution: crossover

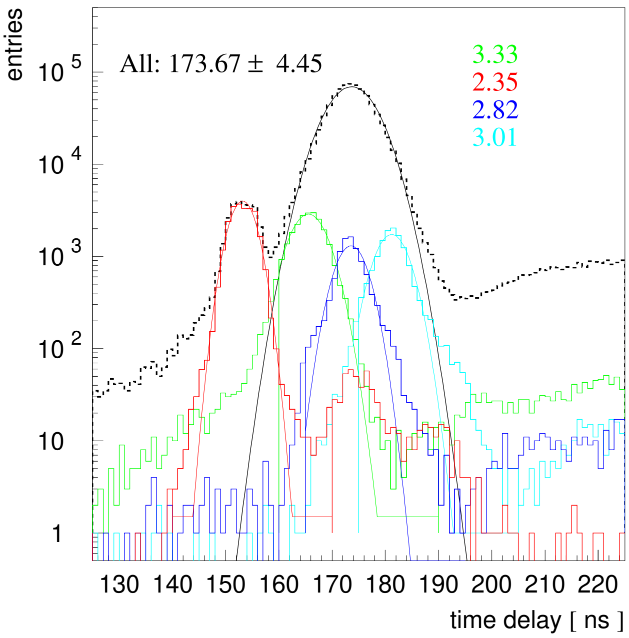

Figure 20: Laser time resolution: le threshold

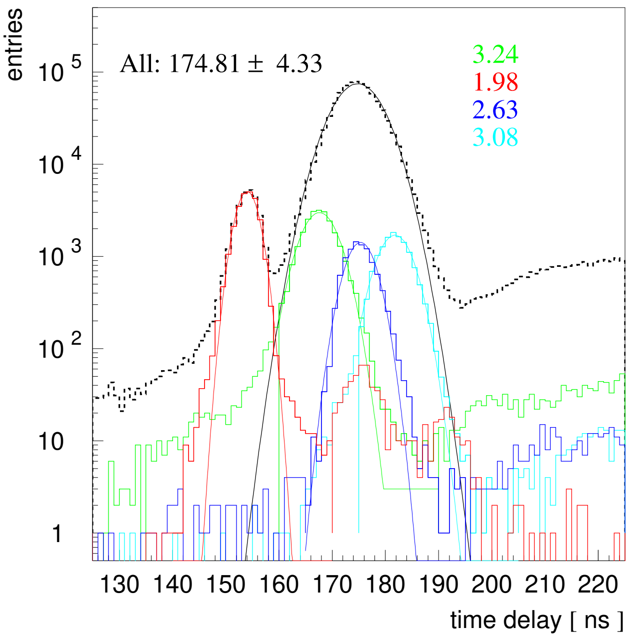

Figure 21: Laser time resolution: le intercept

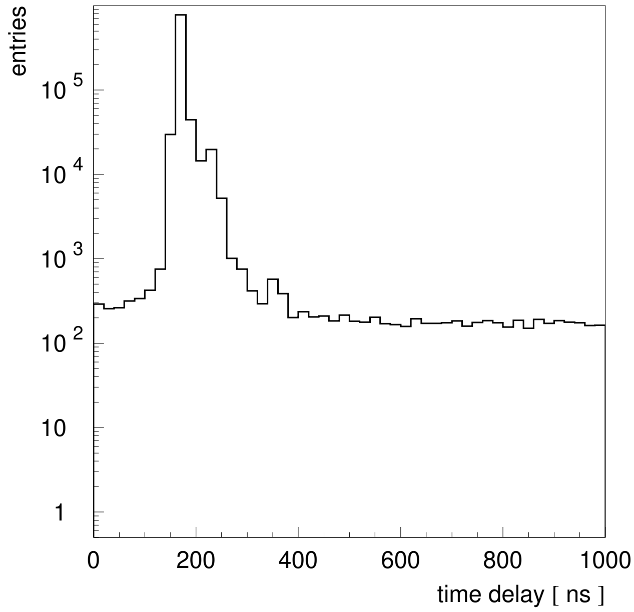

Figure 22: PMT pulse time correlation with the laser pulse

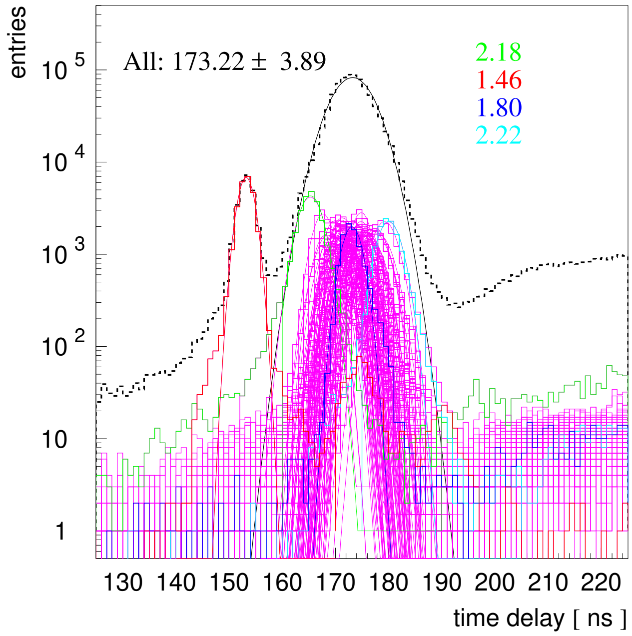

Figure 23: Laser time resolution: crossover

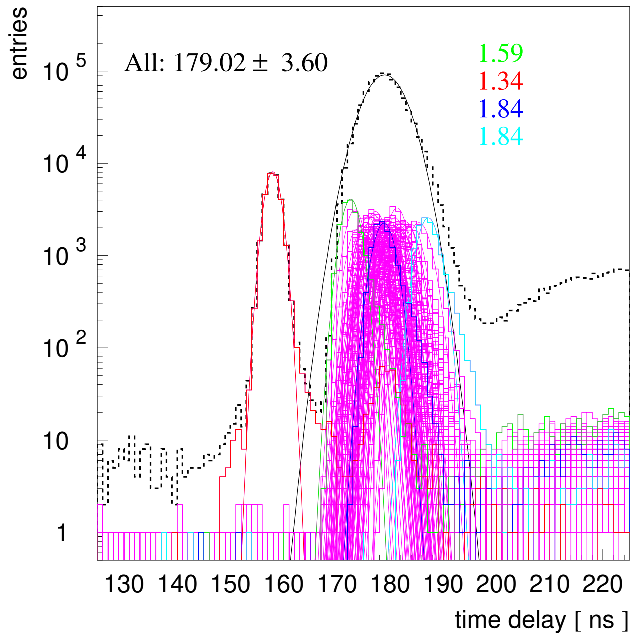

Figure 24: Laser time resolution: crossover, hit cleaning (including the 2 ns time mismatch cut)

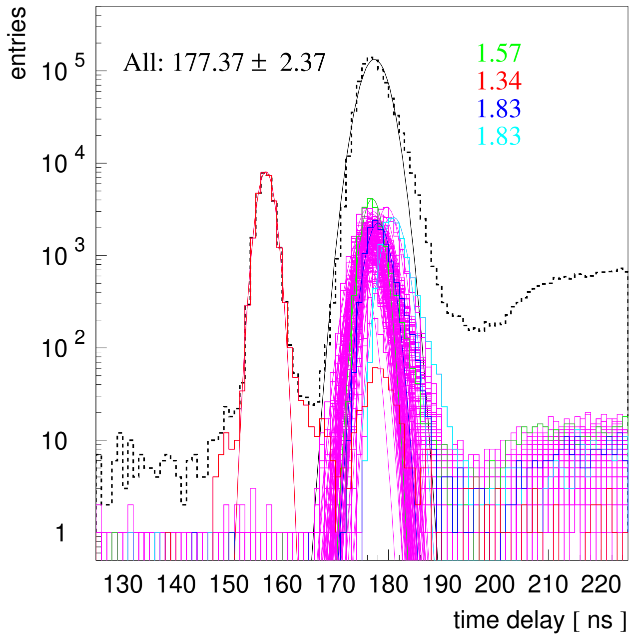

Figure 25: Laser time resolution: crossover, hit cleaning, t_0 vs. waveform width correction, high voltage vs. t_0 correction

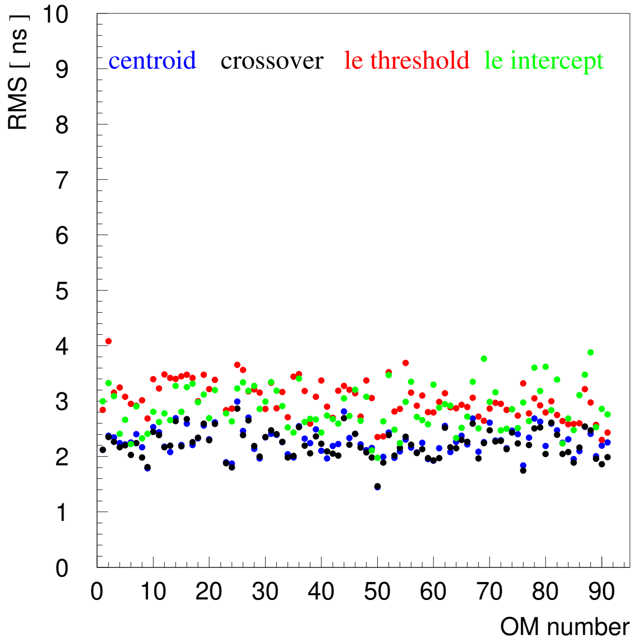

Figure 26: RMS of the laser t_0 measurement

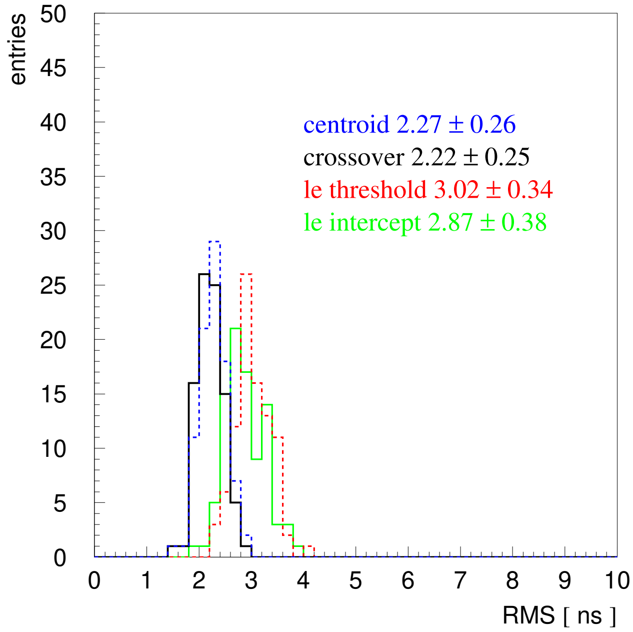

Figure 27: Distribution of the DOM time resolution

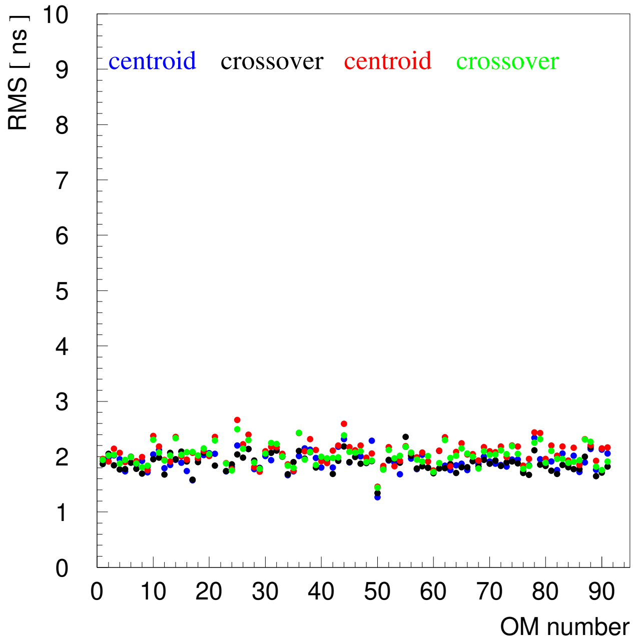

Figure 28: RMS of the laser t_0 measurement, hit cleaning

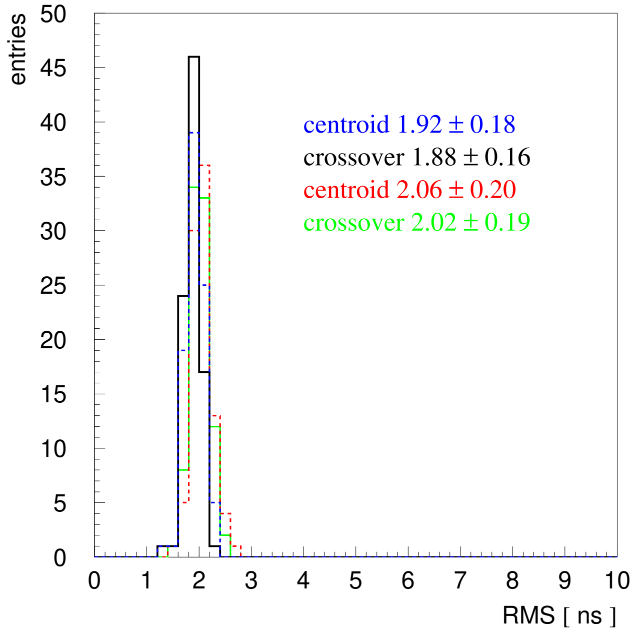

Figure 29: Distribution of the DOM time resolution, hit cleaning

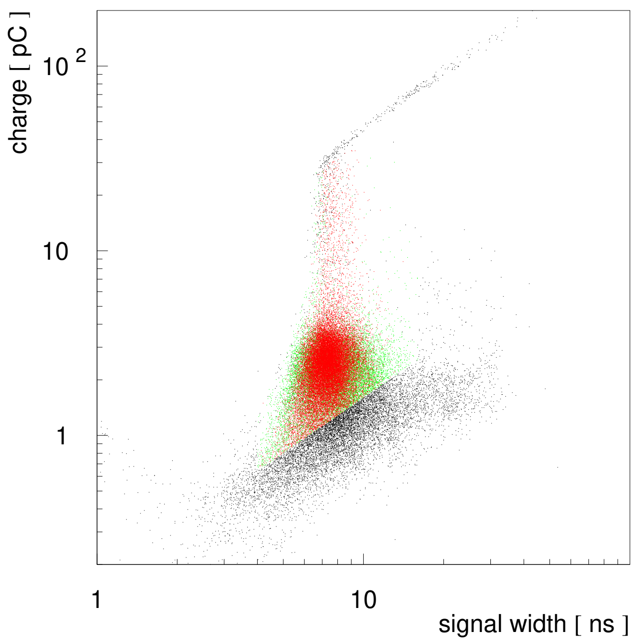

Figure 30: Waveform charge vs. signal width

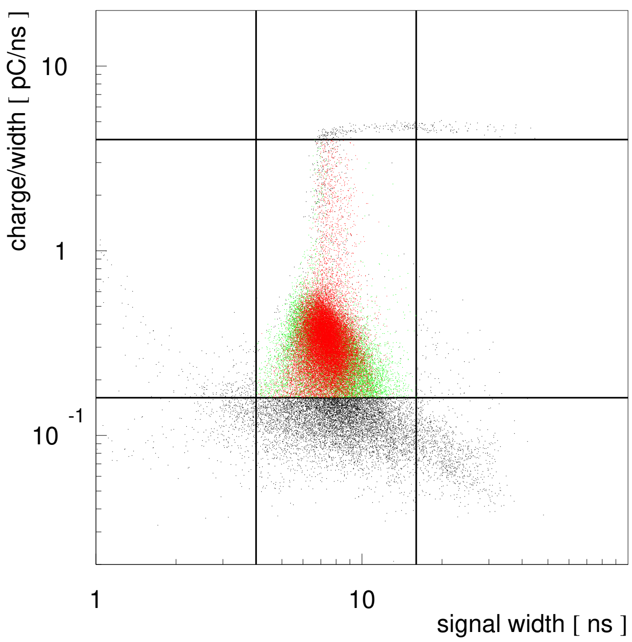

Figure 31: Noise and saturated pulse cleaning cuts

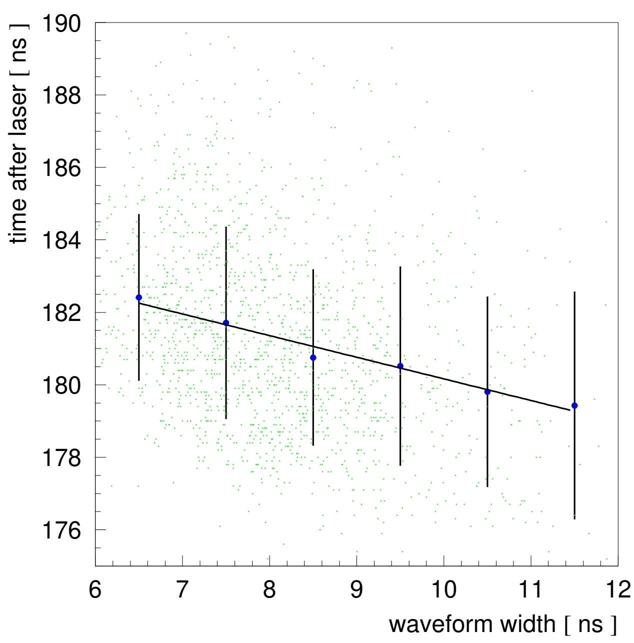

Figure 32: t_0 vs. waveform width correlation

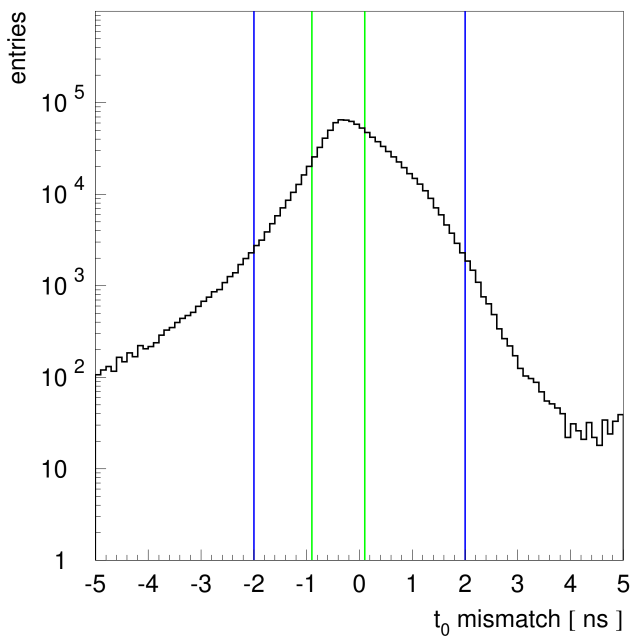

Figure 33: t_0 mismatch distribution and cuts

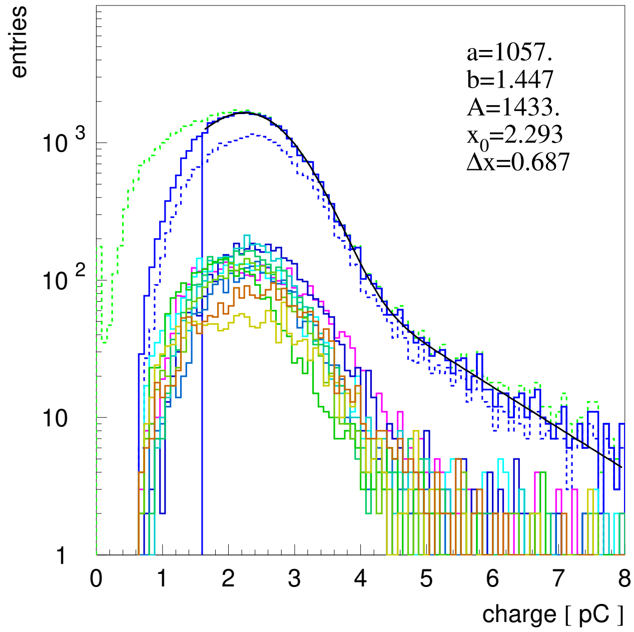

Figure 34: 1 pe pulse charge distribution: dashed green: all, solid blue: hit cleaning, dashed blue: also t_0 mismatch cleaning (< 2 ns)

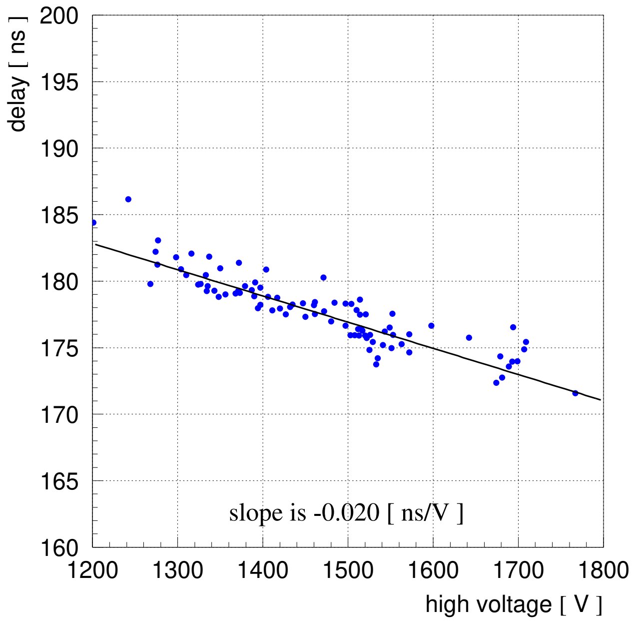

Figure 35: PMT high voltage vs. t_0 correlation

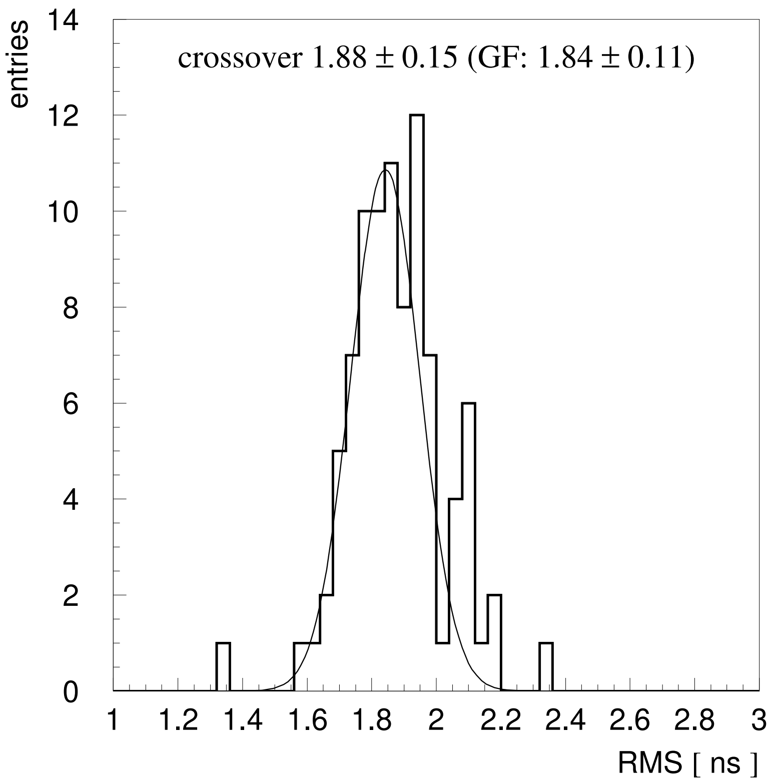

Figure 36: Laser time resolution: best result

A.5 Final acceptance test (FAT) data reader software

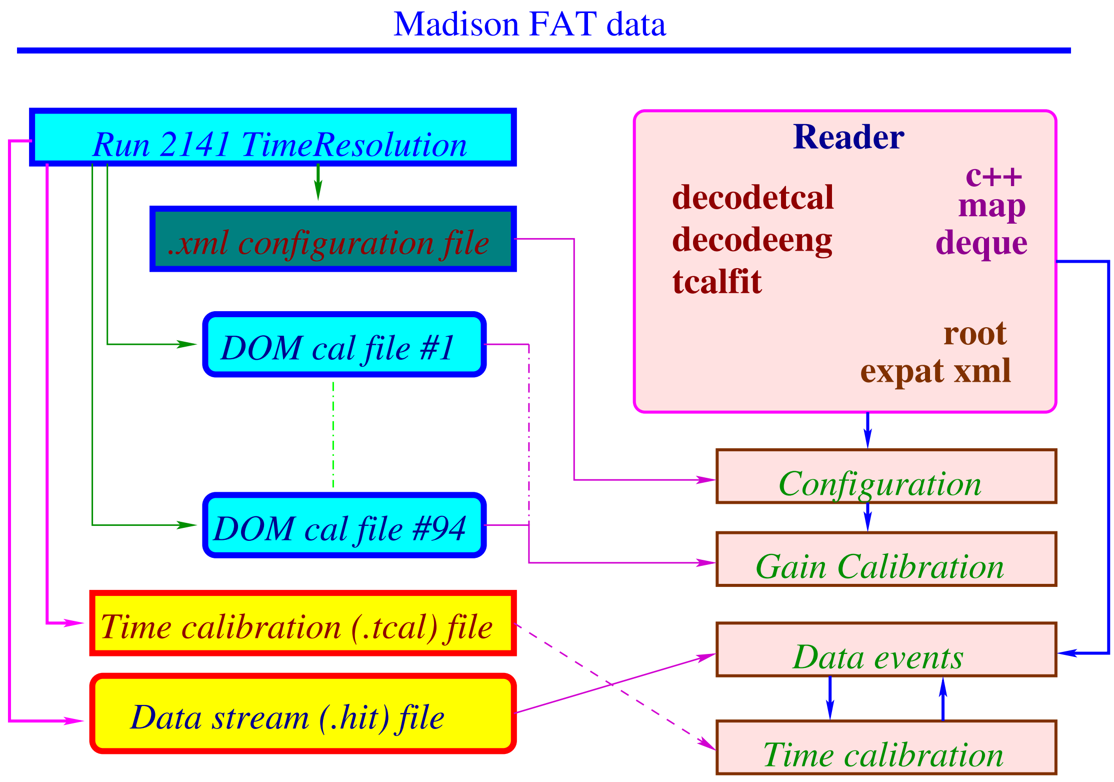

Figure 37: Reader program structure

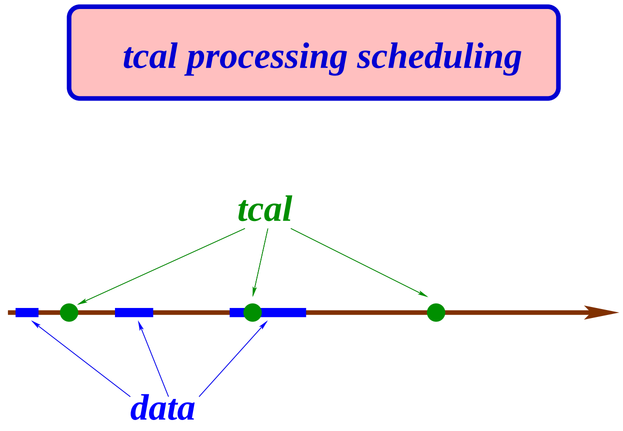

Figure 38: Tcal cycle scheduling during data taking

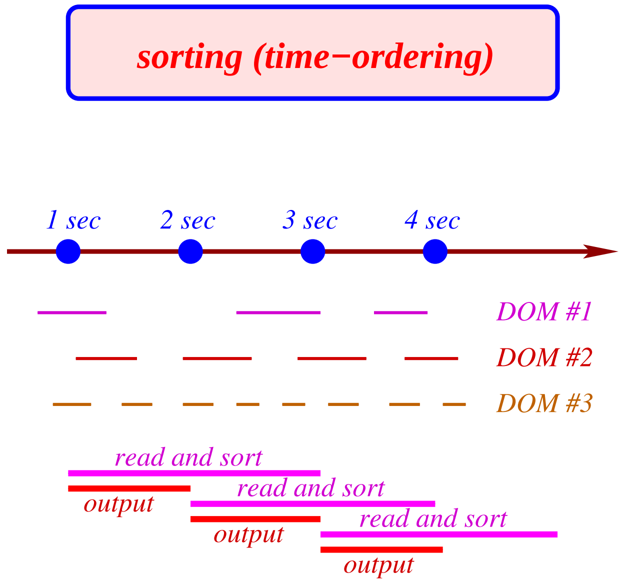

Figure 39: Event time-ordering